Journal of Applied Mathematics and Physics, 2024, 12, 3037-3052
https://www.scirp.org/journal/jamp
ISSN Online: 2327-4379
ISSN Print: 2327-4352

Hybrid Effects on MHD Mixed Convective Boundary Layer Flow through a Sloped Plate in Existence of Nanofluid-Saturated Porous Medium

Md. Nasir Uddin[1*], Abdul Halim Bhuiyan[2], Zahurul Islam[1], Tahmina Tahrim[3]

[1]Department of Mathematics, Bangladesh Army University of Engineering & Technology, Natore, Bangladesh
[2]Department of Mathematics, Bangladesh University of Engineering and Technology, Dhaka, Bangladesh
[3]Department of Computer Science and Engineering, Jagannath University, Dhaka, Bangladesh
Email: *mnasiruddin07@gmail.com

How to cite this paper: Uddin, Md.N., Bhuiyan, A.H., Islam, Z. and Tahrim, T. (2024) Hybrid Effects on MHD Mixed Convective Boundary Layer Flow through a Sloped Plate in Existence of Nanofluid-Saturated Porous Medium. *Journal of Applied Mathematics and Physics*, **12**, 3037-3052.
https://doi.org/10.4236/jamp.2024.129182

Received: August 7, 2024
Accepted: September 3, 2024
Published: September 6, 2024

Abstract

This study examines the effects of heat, mass, and boundary layer assumptions-based nanoparticle characteristics on the hybrid effects of using MHD in conjunction with mixed convective flow through a sloped vertical pore plate in the existence of medium of porous. Physical characteristics such as thermo-diffusion, injection-suction, and viscous dissipation are taken into consideration, in addition to an equally distributed magnetic force utilized as well in the completely opposite path of the flow. By means of several non-dimensional transformations, the momentum, energy, concentration, and nanoparticle volume fraction equations under investigation are converted in terms of non-linear boundary layer equations and computationally resolved by utilizing the sixth-order Runge-Kutta strategy in combination together with the iteration of Nachtsheim-Swigert shooting procedure. By contrasting the findings produced for a few particular examples with those found in the published literature, the correctness of the numerical result is verified, and a rather good agreement is found. Utilizing various ranges of pertinent factors, computing findings are determined not only regarding velocity, temperature, and concentration as well as nanoparticle fraction of volume but also concerning with local skin-friction coefficient, local Nusselt and general Sherwood numbers associated with nanoparticle Sherwood number. The findings of the study demonstrate that increasing the fluid suction parameter decreases the velocity and temperature of the flow field in conjunction with concentration and has a variable impact on the nanoparticle fraction of volume, despite an increasing behavior in the local skin friction coefficient and local Nusselt as well as

general Sherwood numbers and an increasing behavior in the local nanoparticle Sherwood number. Furthermore, enhancing a Schmidt number leads to a reduction in the local nanoparticle Sherwood number and a rise in the nanoparticle proportion of volume. Along with concentration, it also reduces temperature and velocity. However, it also raises the local Sherwood and Nusselt numbers and reduces the local skin friction coefficient.

Keywords

Hybrid Effects, Mixed Convection, MHD, Nanofluid, Viscous Dissipation

1. Introduction

Due to the remarkable applications of nanofluid in extensive thoroughness of engineering and applied fields, including electronics, material processing, scientific measurement, computer technologies, high-power X-rays, optical devices, transportation, food, nuclear reactors, medicine, and synthesis, nanofluids have garnered a great deal of attention in research over the past ten years. Nanofluids have recently been explored as a means of improving thermal conductivity and comprehending their behavior, which will enable their use in numerous applications where improving straight heat transmission is crucial.

For mass, momentum, and heat transport in nanofluids, Buongiorno [1] has devised a two-component, four-equation nonhomogeneous equilibrium model. Abu-Nada [2] has studied heat transmission across a backward-facing stair using nanofluids. It has been found that high thermal conductivity nanoparticles exhibit greater increases on the Nusselt number outside of the circulation regions. However, low-thermal conductivity nanoparticles have superior heat transfer increases within the primary and secondary recirculation zones. Convection in a horizontal tier in porous material inclusive of nanofluid-saturated has been investigated via Nield and Kuznetsov [3]. In their investigation, they have taken thermophoresis and Brownian motion into account. In presence of nanofluids, they also discovered that there could be a substantial rise or fall in the crucial thermal Rayleigh number. Furthermore, The Cheng-Minkowycz scenario, which involves convective boundary tier flow across a perpendicular wall in a nanofluid-saturated medium with pores, has been analytically explored by Nield and Kuznetsov [4]. They offered a similar solution after predicting when nanofluid convection will begin using the Darcy model. Employing a variety of nanofluid types, including Cu, Al_2O_3, and TiO_2, Ahmad and Pop [5] have analytically explored the diverse convective flow of boundary tier across the vertical plain wall inserted into a medium composed of pores that is filled using nanofluids. A computational analysis comprising diverse convection in an environment composed of pores occupied by Al_2O_3 and water has been carried out by Mittal *et al.* [6].

Results for several parameters were shown graphically and tabulated, and a discussion followed. Yasin *et al.* [7] have explored numerically the continuous

diverse convective flow of boundary tier across a vertical surface into an environment composed of pores that is filled using nanofluids. In a water-based nanofluid, they employed dissimilar categories of metallic or nonmetallic nanoparticles, such as titania (TiO_2), alumina (Al_2O_3), and copper (Cu) to examine the impact of the nanofluid's solid volume fraction characteristic upon the heat transmission as well as flow properties. The temperature distributions, velocity, and skin friction coefficient were all shown and discussed afterward. They came to the conclusion that a major element in the improvement of heat transmission is the type of nanofluid. Gorla and Hossain [8] have looked into the impacts of Brownian motion as well as thermophoresis on a boundary layer analysis on an isothermal vertical cylinder within an environment composed of pores saturated by nanofluid involving mixed convection. In the boundary layer, they found that the thermophoresis parameters, buoyancy ratio, and Brownian motion had a significant impact on the rate of mass in conjunction with heat transfers.

In the context of an expanded annulus enclosure comprised of pore materials, Saleh [9] has computationally explored the natural convection process regarding nanofluid heat transfer involving a pair of horizontal concentric cylinders by employing the twelve annular fins of 2.4 mm depth connected with an inside cylinder according to constant-state circumstances. Copper (Cu) was used as the nanoparticle. Uddin and Harmand [10] have developed the Darcy-Forchheimer model to describe the irregular natural convective heat transfer flow of nanofluid over an isothermal vertical plate placed within an environment of pore medium. They discovered the fact that rather than the composition of the additional nanoparticles, the primary factor affecting heat transfer in nanofluids is the character underlying the base fluid. In environments where convection is fueled by two distinct density gradients with varying rates of diffusion, such as oceans and magma chambers, double-diffusion is a significant topic in fluid dynamics occurs. The implications of the considerable Soret reaction on mass transfer as well as double-diffusive natural convection heat in the boundary tier area associated with a semi-infinite sloped plane plate within a medium of pores that is non-Darcy and saturated with nanofluids have been addressed by Murthy *et al.* [11]. They found that greater Soret parameter values increase the mass transfer rates of heat and nanoparticles but decline the regular mass transfer rate at boundary.

Achieving balance or the desired control over the flow has been facilitated by a uniform distribution of the magnetic force in the opposite direction of the flow. In applications such as magnetic flow control or stabilization, it indicates that the magnetic force has successfully opposed the flow to produce stability or control. However, complex interactions between the magnetic forces and the fluid dynamics have been introduced by varying magnetic force distributions. This can impact the system's overall efficacy or efficiency and require the use of more complex models to precisely forecast the flow behavior. The impacts of both viscous dissipation as well as the field of magnetic attraction on free convective mass and heat transport over a vertical plate within a medium of pores that is non-Darcy and saturated with nanofluids have been deliberated via Reddy *et al.* [12]. The authors

found that while the rate of nanoparticle mass transfer and temperature in conjunction with velocity distributions were improved via increasing the viscous dissipation parameter, the heat transfer rate in association with distribution of fraction of nanoparticle volume was decreased. Furthermore, lower velocity distributions, mass and heat transfer rates for nanoparticles, in addition to higher volume fraction and temperature distributions for nanoparticles, are the outcomes of higher magnetic parameter values. The system relating the flow of mixed convective boundary layer over a sloped plate in a nanofluid-saturated pores medium filled with has been explained using double distinct analytical and numerical methods, the Chebyshev Pseudo-Spectral Differentiation Matrix and the Homotopy Perturbation Method, as studied by Aly and Ebaid [13]. Employing a range of values of the relevant physical features, the temperature and nanoparticle concentration distributions' numerical results have been shown by them. Yazdi *et al.* [14] have explored the two-dimensional mixed convective magnetohydrodynamic boundary layer characterized by stagnation-point flow in the existence of heat radiation through a stretching vertical plate within an environment of porous medium containing a nanofluid.

As one gets farther away of the stagnation point, it is thought that the stretching velocity as well as surrounding fluid velocity varies linearly. With copper serving as the base fluid of the aiding as well as opposing flows, the findings have been presented for three distinct nanoparticle categories: copper, titania, and alumina. It has been studied by Srinivasacharya and Surender [15] how solutal together with thermal stratifications affect diverse convective boundary layer flow along a plate that is vertically placed within a porous medium containing nanofluid. They suggested that increasing the thermal as well as solutal stratification parameters causes the temperature to drop but the concentration to rise. Additionally, they provided a graphic representation of how mass transfer features and heat, in conjunction with velocity varied depending on distinct physical parameters. Employing on boundary layer approximations, El-Dawy *et al.* [16] have reported mixed convection via a vertical plate in a nanofluid-saturated medium of pores. The rate of surface heat transfers and friction factor in terms of numerical results are shown, along with the variations of the buoyancy ratio parameter, viscosity, and Prandtl number in conjunction with nanoparticle volume percentage.

Moreover, MHD flow involving mass transfer and nanofluid with heat-transfer characteristics across porous medium has been documented by Reddy and Chamkha [17]. For non-Newtonian fluid, Khan *et al.* [18] have reported, in conjunction with uniform fluid suction, the effect of thermal radiation as well as chemical reactions regarding the unsteady flow by way of a vertically stretching porous plate. They discovered that within the boundary tier, the temperature profiles are higher with respect to the heat source parameter as well as lower on account of the heat sink parameter. Within a substance with pores surrounding an accelerating vertically wavy plate, the influence of Soret regarding unsteady MHD diverse convective transfer of mass as well as heat flow has been explored via Prasad *et al.* [19], considering thermal radiation, chemical reaction, angle of inclination, heat

generation, and Casson fluid. The diverse convective fluid flow of nanofluid across and through a medium with pores utilizing a sloped pore plate has been examined by Uddin *et al.* [20], reasoning that the magnetic field has unique impacts on viscous dissipation. This work has the potential to be expanded by utilizing the unique characteristics of thermophoretic velocity in addition to chemical reactions concerning concentration for various kinds of nanofluid flow. By Falodun *et al.* [21], the Cattaneo-Christov model has been utilized to explore the importance of viscous dissipation, thermal radiation, as well as heat generation for a hybrid MHD flow. Utilizing a constant heat source, radiation absorption, an inclined porous vertical plate positioned inside a media with pores, and changing circumstances at the boundary, Raghunath *et al.* [22] have investigated the chemical reaction as well as diffusion thermos consequences for the natural convective transfer of double diffusive flow of Jeffrey nanofluids.

As previously indicated, it makes more sense to look into how momentum features, together with mass as well as heat transfer, and the properties of nanoparticles, affect mixed convective flow through a vertically sloped porous plate within an environment of nanofluid-saturated medium of pores employing boundary-layer approximations. The significant geometries and the impacts described have not yet been investigated, to the greatest extent of the author's understanding. This study has significant applications in various fields, including petroleum engineering, aerospace engineering, and the cooling of electronic equipment. Additionally, it plays a crucial role in enhancing nuclear reactor safety and has the potential to benefit many other areas as well.

2. Formulation of Mathematical Modeling

The study investigates the interaction of two-dimensional mixed convective flow with magnetohydrodynamics (MHD) passing through a porous plate sloped at an exquisite angle α relative to the vertical direction. More than that, the fluid is recognized a stable, viscous, and incompressible electrically conducting fluid. The physical parameters y and x are selected to be such a way that y is obtained perpendicular towards the sloped porous plate while x is obtained streamwise as of the edge that leads. Moreover, v and u, respectively, are the components of velocity that perpendicular and in the path of the flow. On the other hand, a field of magnetic B_0 in a steady condition that is acted to the path of normal of flow and g is the force of gravity generates acceleration. An external flow characterized by a uniform velocity U_∞ directed parallel to the sloped porous plate is present. Let ϕ, C, and T indicate in terms of the fluid's volume fraction of nanoparticles, concentration, and temperature, correspondingly.

The ambient temperature T_∞ and concentration C_∞ as well as the nanoparticle volume fraction ϕ_∞ are less than those relating to the wall temperature T_w and concentration C_w as well as the nanoparticle volume fraction ϕ_w, respectively. Figure 1 presents a schematic perspective of the coordinate system and flow setup below.

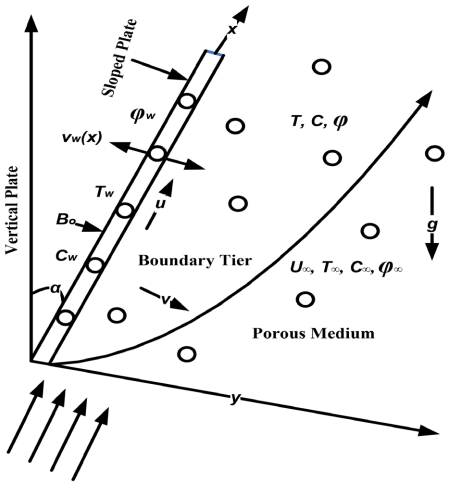

Figure 1. The Graphic perspective of coordinate system together with flow setup.

Consistent, two-dimensional, laminar boundary layer flow is deliberated as a result of the following equations utilizing the aforementioned characteristics:

$$\frac{\partial u}{\partial x}+\frac{\partial v}{\partial y}=0 \tag{1}$$

$$\begin{aligned} u\frac{\partial u}{\partial x}+v\frac{\partial u}{\partial y}=\nu\frac{\partial^2 u}{\partial y^2}+g\left(T-T_\infty\right)\beta_T\cos\alpha+g\left(C-C_\infty\right)\beta_C\cos\alpha \\ +g\left(\phi-\phi_\infty\right)\beta_N\cos\alpha-\left(\frac{\sigma B_0^2}{\rho}+\frac{\nu}{k^*}\right)u \end{aligned} \tag{2}$$

$$u\frac{\partial T}{\partial x}+v\frac{\partial T}{\partial y}=\frac{k}{\rho C_p}\frac{\partial^2 T}{\partial y^2}+\frac{Q_0}{\rho C_p}\left(T-T_\infty\right)+\frac{\sigma B_0^2}{\rho C_p}u^2 \tag{3}$$

$$u\frac{\partial C}{\partial x}+v\frac{\partial C}{\partial y}=-\frac{\partial}{\partial y}\left[\left(C-C_\infty\right)V_T\right]+D_M\frac{\partial^2 C}{\partial y^2} \tag{4}$$

$$u\frac{\partial \phi}{\partial x}+v\frac{\partial \phi}{\partial y}=D_B\frac{\partial^2 \phi}{\partial y^2}+D_T\frac{\partial^2 T}{\partial y^2} \tag{5}$$

within the aforementioned equations, ν denotes the kinematic viscosity, k^* denotes the permeability of the porous medium, σ represents the electrical conductivity, ρ designates density, and k indicates thermal conductivity of the fluid. For a comprehensive understanding of the governing equations, one may review the works of Buongiorno [1], Nield and Kuznetsov [4], and Murthy *et al.* [11].

Additionally, β_C, β_T, and β_N are the volumetric coefficients of mass fraction, thermal expansion, and nanoparticle fraction, respectively. It is possible to express that the Brownian and thermophoretic diffusion coefficients are D_B and D_T, whereas the mass diffusivity is D_M and the specific heat at constant pressure is C_p, the heat generation constant is Q_0 and the thermophoretic velocity is well-defined by

$$V_T=-\frac{\upsilon\kappa}{T_{ref}}\frac{\partial T}{\partial y} \tag{6}$$

wherein κ is the coefficient of thermophoretic, which is calculated as follows by Talbot *et al.* [23] and T_{ref} is some reference temperature as:

$$\kappa = \frac{2C_s\left(\frac{k_g}{k_p}+C_t k_n\right)\left\{1+k_n\left(C_1+C_2 e^{-\frac{C_3}{k_n}}\right)\right\}}{\left(1+2C_t k_n+2\frac{k_g}{k_p}\right)\left(1+3C_m k_n\right)} \tag{7}$$

where k_n represents the Knudsen number, k_g and k_p represent the fluid's and the disseminated particle's respective thermal conductivities, and C_t, C_s, C_m, C_1, C_2, and C_3 are constants.

The following are the suitable boundary conditions for this consideration's temperature, velocity, concentration, and volume fraction of nanoparticles:

$$u=0,\ v=\pm V_w(x),\ T=T_w,\ C=C_w \text{ and } \phi=\phi_w \text{ at } y=0 \tag{8}$$

$$u=U_\infty,\ T=T_\infty,\ C=C_\infty \text{ and } \phi=\phi_\infty \text{ as } y\to\infty \tag{9}$$

Furthermore, the porous plate's permeability is denoted by $V_w(x)$, whose sign designates either blowing (>0) or suction (<0), and the free stream velocity is represented by U_∞. The subscripts w as well as ∞, correspondingly, indicate the boundaries of the wall as well as the boundary layer. For the purpose of facilitating the analysis, the dimensionless components established by Cebeci *et al.* [24] are incorporated, so the differential equations that govern the analysis are rendered nondimensional through the appropriate transformations:

$$\begin{aligned}&\eta = y\left(\frac{U_\infty}{x\nu}\right)^{\frac{1}{2}},\ \psi=\left(x\nu U_\infty\right)^{\frac{1}{2}} f(\eta),\ \theta(\eta)=\frac{T-T_\infty}{T_w-T_\infty},\\ &s(\eta)=\frac{C-C_\infty}{C_w-C_\infty} \text{ and } \gamma(\eta)=\frac{\phi-\phi_\infty}{\phi_w-\phi_\infty}\end{aligned} \tag{10}$$

in which $\psi(x,y)$ is the stream function that is automatically satisfied by Equation (1) for continuity and is determined through:

$$\frac{\partial\psi}{\partial y}=u \text{ and } -\frac{\partial\psi}{\partial x}=v \tag{11}$$

These new variables allow us to express the velocity components as follows:

$$u=U_\infty f'(\eta) \text{ and } v=\frac{1}{2}\left(\frac{\nu U_\infty}{x}\right)^{\frac{1}{2}}\left\{-f(\eta)+\eta f'(\eta)\right\} \tag{12}$$

In this case, the prime denotes usual differentiation on the subject of similarity variable η. Corresponding modified equations for momentum, energy, concentration, and nanoparticle volume fraction, together with associated boundary situations, can be embodied as follows using dimensionless variables:

$$\begin{aligned}&f'''(\eta)+0.5 f(\eta) f''(\eta)+\left\{R_{it}\theta(\eta)+R_{ic}s(\eta)+R_{in}\gamma(\eta)\right\}\cos\alpha\\ &-\left(K+M_1\right) f'(\eta)=0\end{aligned} \tag{13}$$

$$\theta''(\eta)+Pr\left\{0.5f(\eta)\theta'(\eta)+Q\theta(\eta)+EcM_2f'^2(\eta)\right\}=0 \tag{14}$$

$$s''(\eta)+Sc\left[0.5f(\eta)s'(\eta)-\tau\left\{s'(\eta)\theta'(\eta)+s(\eta)\theta''(\eta)\right\}\right]=0 \tag{15}$$

$$\gamma''(\eta)+0.5Sc_nf(\eta)\gamma'(\eta)+N\theta''(\eta)=0 \tag{16}$$

and under the boundary circumstances:

$$f=f_w,\ f'=0,\ \theta=1,\ s=1, \text{ and } \gamma=1 \text{ at } \eta=0 \tag{17}$$

$$f'\to 1,\ \theta\to 0,\ s\to 0, \text{ and } \gamma\to 0 \text{ as } \eta\to\infty \tag{18}$$

Here, however, $f_w<0$ indicates wall injection but $f_w>0$ designates wall suction, according to the wall mass transfer coefficient:

$$f_w=-V_w(x)\sqrt{\frac{x}{\nu U_\infty}} \tag{19}$$

The definition of the associated dimensionless groups that show up in the governing equations' nondimensional version consists of the following:

$$\begin{aligned}&R_{it}=\frac{Gr_t}{(Re)^2},R_{ic}=\frac{Gr_c}{(Re)^2},R_{in}=\frac{Gr_n}{(Re)^2},M_1=M_2=\frac{\sigma B_0^2x}{\rho U_\infty},K=\frac{\nu x}{k^*U_\infty},\\&Pr=\frac{\nu\rho C_p}{k},Q=\frac{xQ_0}{\rho C_pU_\infty},Ec=\frac{U_\infty^2}{C_p(T_w-T_\infty)},Sc=\frac{\nu}{D_M},\\&\tau=-\frac{K}{T_{ref}}(T_w-T_\infty),Sc_n=\frac{\nu}{D_B}\text{ and }N=\frac{D_T}{D_B}\frac{(T_w-T_\infty)}{(\phi_w-\phi_\infty)}\end{aligned} \tag{20}$$

where the local Grashof numbers are Gr_t for local thermal Grashof, Gr_n for local nanoparticle Grashof, Gr_c for local mass Grashof, Re for local Reynolds, and R_{it} for local thermal Richardson, R_{ic} for local mass, and R_{in} for local nanoparticle Richardson. The parameters that are shown are as follows: M stands for magnetic field, K for permeability, Ec for Eckert number, Q for heat generation, Pr for Prandtl number, and Sc for Schmidt number, τ for thermophoretic parameter, Sc_n for nanoparticle Schmidt number, then N for modified nanoparticle parameter.

Utilizing the wall shear stress definition $\tau_w=\mu\left(\frac{\partial u}{\partial y}\right)_{y=0}$ in conjunction with Fourier's law $q_w=-k\left(\frac{\partial T}{\partial y}\right)_{y=0}$, Fick's law $q_m=-D_M\left(\frac{\partial C}{\partial y}\right)_{y=0}$, and $q_{np}=-D_B\left(\frac{\partial\phi}{\partial y}\right)_{y=0}$, it is possible to determine the nondimensional forms of $C_f=2(Re)^{-\frac{1}{2}}f''(0)$ as local skin-friction coefficient, $N_u=-(Re)^{\frac{1}{2}}\theta'(0)$ as local Nusselt number, $S_h=-(Re)^{\frac{1}{2}}s'(0)$ as local Sherwood number, and $S_{hn}=-(Re)^{\frac{1}{2}}\gamma'(0)$ as local nanoparticle Sherwood number as well as their corresponding nondimensional forms. However, the local Reynolds number stands for $Re=\frac{xU_\infty}{\nu}$.

3. Numerical Approach for Solution

The transferred governing equations can be solved using several different tactics. Utilizing the appropriate similarity transformations, non-linear equations of operation are first converted as contemporaneous ordinary differential equations. The boundary value problem is subsequently further converted as the initial value problem through the above equations employing Nachtsheim and Swigert's shooting technique [25]. Utilizing the Runge-Kutta sixth-order approach, the resulting initial value problem is resolved.

The local skin-friction coefficient, local Nusselt number, and local general together with nanoparticle Sherwood numbers are computed from the numerical process of computation, and their numerical values are graphically presented. Additionally, the fields of velocity, concentration and nanoparticle volume fraction as well as the temperature are incorporated. The leading numerical tactic is reference to Nachtsheim and Swigert [25], which are included throughout the detailed description of the numerical approaches.

4. Validation of the Model

The current work, which does not use a nano-particle equation, is contrasted to the earlier released research by Reddy and Reddy [26] for the purpose of assessing the accuracy of the computational findings, as seen in **Figure 2** below. The velocity distribution of Reddy and Reddy [26] and the current numerical results are shown to have a favorable correspondence in **Figure 2**. The next sections lead to show and analyze the numerical data as a result of this positive comparison.

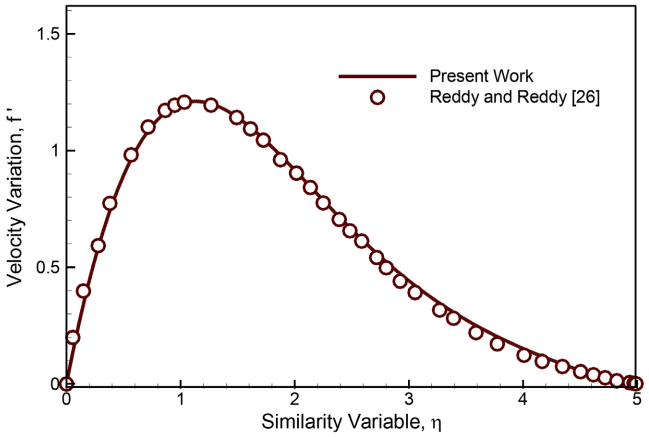

Figure 2. Similarity among the variation in velocity employed in $R_{in} = 0$, $Q = 0.5$, $K = 0.5$, $R_{it} = Gr_t = 2$, $R_{ic} = Gr_m = 2$, $M = M_1 = 0.5$, $M_2 = 0$, $\alpha = 30^0$, $f_w = 0$, $Ec = 0$, $Pr = 0.71$, and $Sc = 0.6$.

5. Findings and Discussions

A comprehensive collection of numerical outcomes derived from the solution of usual differential equations that are nonlinear is visually displayed. Diverse values associated with the corresponding physical parameters are used to obtain the

numerical outcomes due to the distributions of local skin friction in conjunction with the velocity, local Nusselt number in conjunction with temperature, local Sherwood number in conjunction with concentration, and local nanoparticle Sherwood number in conjunction with nanoparticle volume fraction. Unless otherwise noted, $R_{it} = 1$, $R_{ic} = 1$, $R_{in} = 1$, $K = 0.01$, $U_\infty / \nu = 1$, $M_1 = M_2 = 0.02$, $\alpha = 30^\circ$, $Q = 0.5$, $Sc = 0.6$, $Pr = 0.71$, $f_w = 1$, $Ec = 1$, $Sc_n = 0.6$, $N = 0.5$ and $\tau = 0.1$ are the set of deliberated values associated with corresponding numerous physical parameters. It is assumed both the corresponding numerical values for Schmidt number (Sc) in conjunction with Prandtl number (Pr) are 0.6 and 0.71, respectively, for water vapor (H_2O) and air, respectively.

Keeping other flow field parameters constant, **Figure 3** and **Figure 4** show the effects of numerical values 0, 1, and 2 for the suction parameter f_w on the velocity in addition to local skin friction coefficient, temperature in addition to local Nusselt number, concentration in addition to local Sherwood number, and nanoparticle distributions in addition to local Sherwood number of the nanoparticles. **Figure 3(a)** demonstrates that when fluid suction rises, the flow field's velocity drops. This is a result of the plate cooling and the fluid's viscosity rising by means of the fluid suction within the plate rises. As a result, when the fluid suction increases, the flow field's velocity drops. Regarding the temperature variation shown within **Figure 3(b)**, it is discovered when fluid suction is present, the flow field's temperature drops as the plate cools because the flow field produces enhancing fluid suction within the plate. In a similar way, the concentration at all points falls as the fluid suction grows, as can be seen from the concentration variation through **Figure 3(c)**. This happens because increased fluid suction causes the plate to cool.

As the fluid suction is increased, the nanoparticle volume fraction increases at $0 \le \eta < 1.7$ because the difference in volume fraction between the plate and outer edge decreases, and it decreases at $1.7 \le \eta \le 5$ because the wall slope with respect to associated nanoparticle volume fraction increases slightly. This is seen in **Figure 3(d)**. The local skin friction coefficient in addition to the local Nusselt number and the general in addition to nanoparticles local Sherwood numbers are revealed versus the streamwise distance x in **Figure 4**. By means of the fluid suction grows, so too does the local skin friction coefficient C_f, which raises that of the flowing fluid's viscosity as seen in **Figure 4(a)**. However, when the fluid suction parameter rises, the local Nusselt and Sherwood numbers increase as well because of a rise in temperature and concentration variances, correspondingly. These observations can be seen in **Figure 4(b)** and **Figure 4(c)**, while **Figure 4(d)** displays how the local nanoparticle Sherwood number declines.

In order to facilitate the implications of Schmidt number, the corresponding values of Sc are taken as 0.94, 0.60, and 0.22 for carbon dioxide (CO_2), water vapor (H_2O), and hydrogen (H_2), respectively, while maintaining similar values for any other flow field elements. The data laid out in **Figure 5** and **Figure 6** demonstrate the consequences of varying Schmidt numbers Sc on various parameters such as

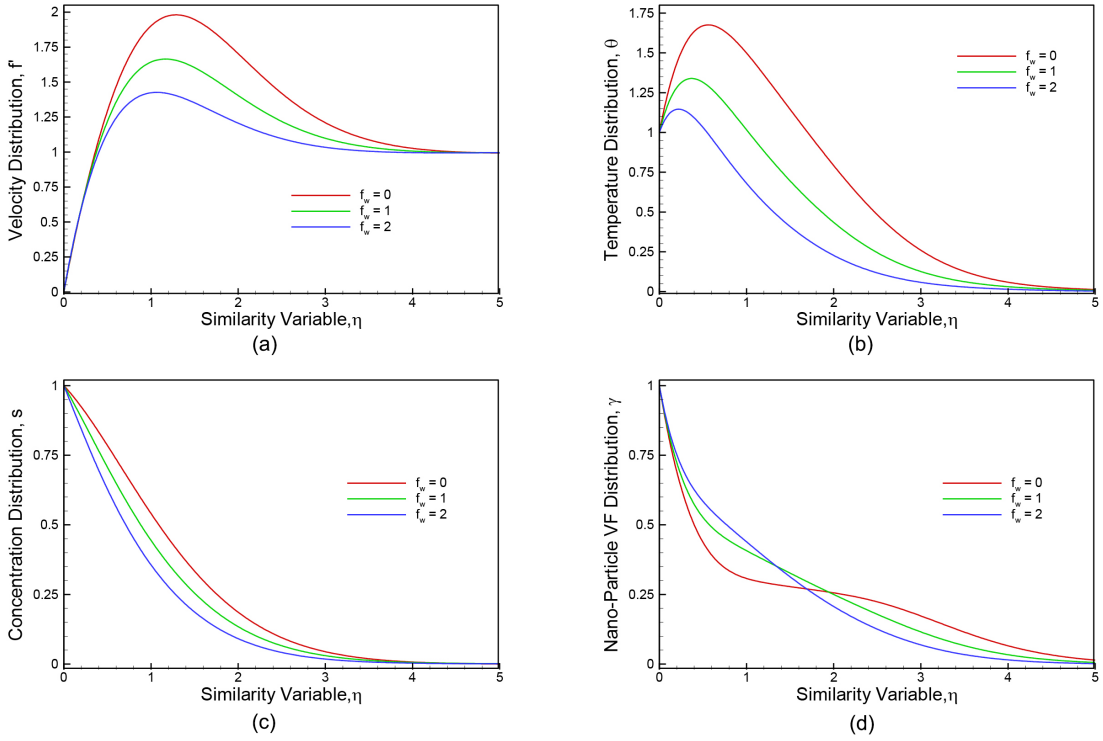

Figure 3. Illustration of (a) velocity, (b) temperature, (c) concentration, and (d) nanoparticle volume fraction variation based on various fluid suction parameter values f_w.

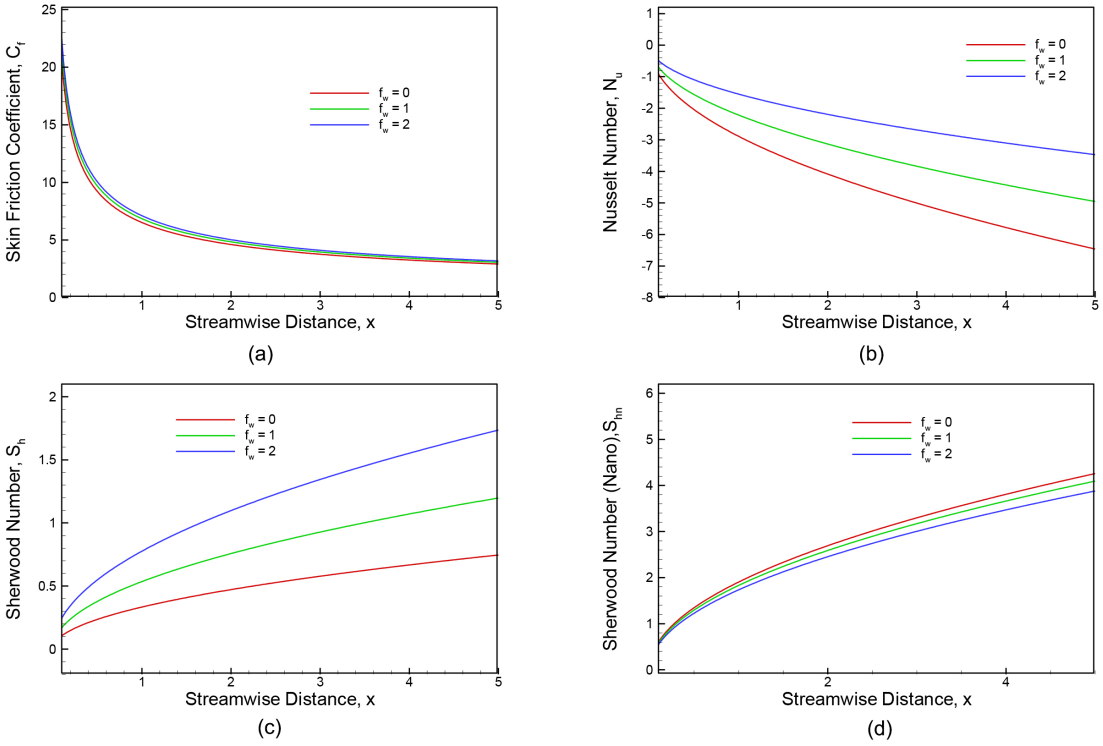

Figure 4. Influence of the fluid suction parameter f_w upon the (a) local skin friction coefficient C_f, (b) local Nusselt number N_u, (c) local Sherwood number S_h, and (d) nanoparticle Sherwood number S_{hn} as a function of the streamwise distance x.

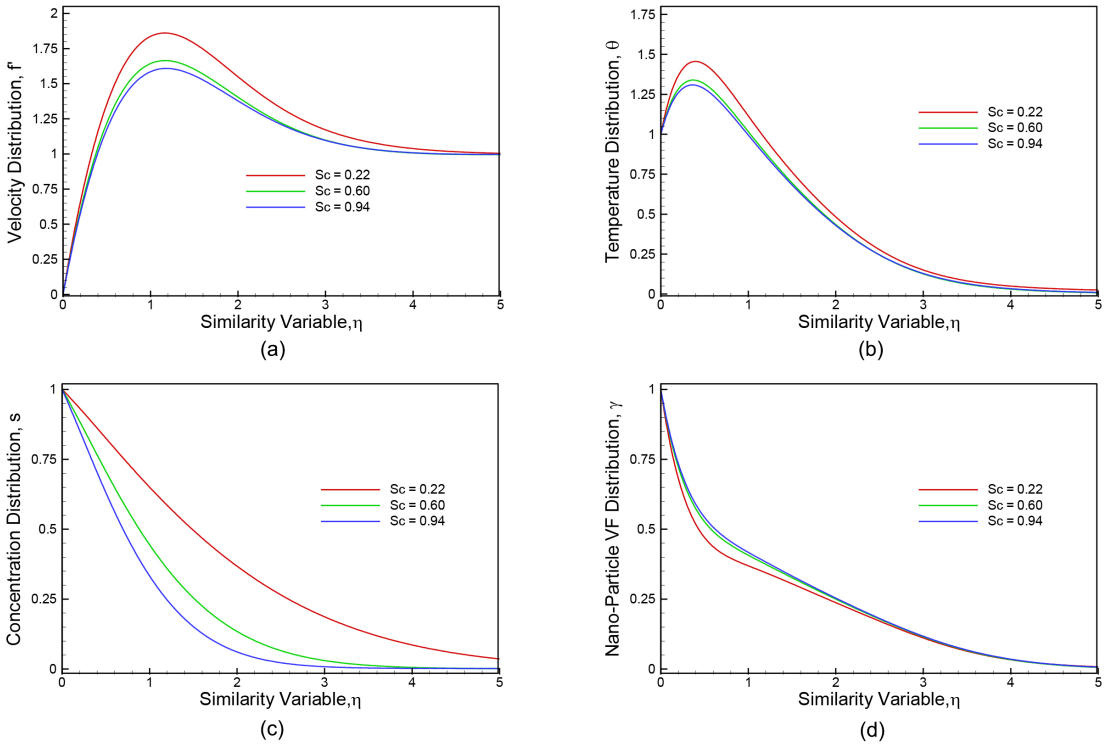

Figure 5. Illustration of (a) velocity, (b) temperature, (c) concentration, and (d) nanoparticle volume fraction variation based on various Schmidt number values *Sc*.

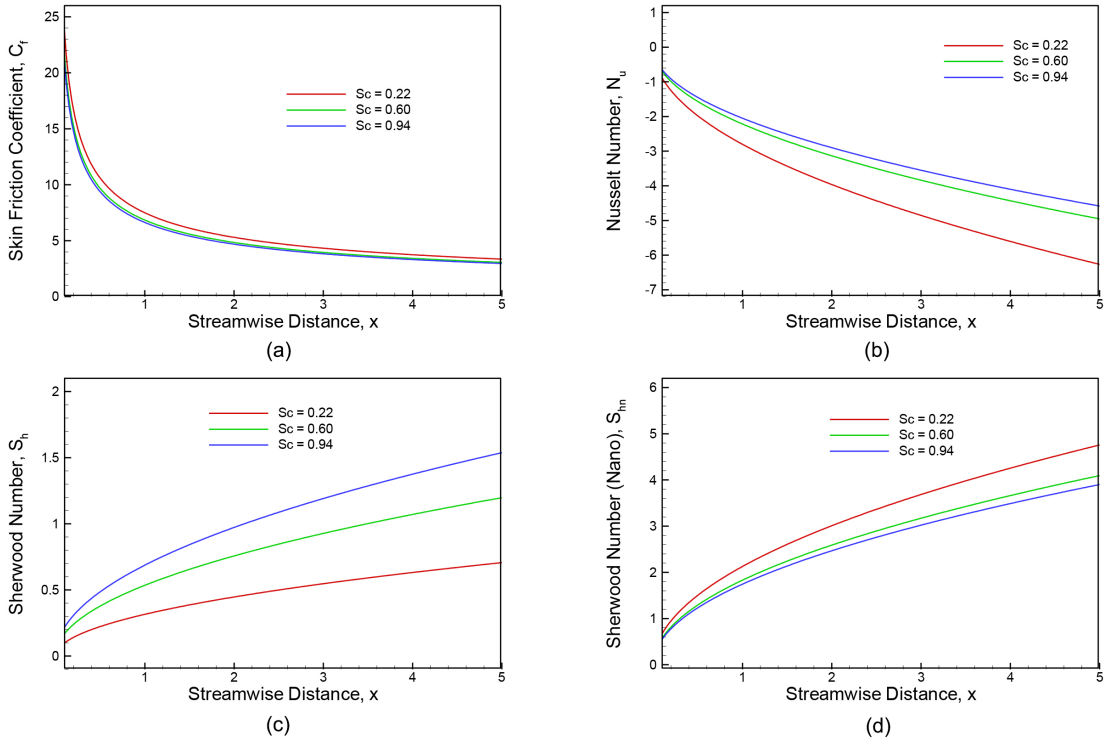

Figure 6. Influence of Schmidt number *Sc* upon the (a) local skin friction coefficient C_f, (b) local Nusselt number N_u, (c) local Sherwood number S_h, and (d) nanoparticle Sherwood number S_{hn} as a function of the streamwise distance *x*.

velocity in addition to local skin friction coefficient, temperature in addition to local Nusselt number, concentration in addition to local Sherwood number, and nanoparticle variation in addition to local nanoparticle Sherwood number in regard to the streamwise distance *x*. The Schmidt number is a ratio of convenient expression for the momentum to diffusivity of mass. Consequently, the Schmidt number is used to quantify the corresponding effectiveness for momentum and mass transmission through diffusion in hydrodynamic and concentration boundary tiers. For the reason of the existence of heavier diffusing species, **Figure 5(a)** demonstrates the manner in which the flow field's velocity drops while the Schmidt number rises. On the contrary, in comparison to the flow field's velocity, the temperature variation—shown in **Figure 5(b)**—varies insignificantly. It is shown that when the diffusing species gets heavier, the flow field's concentration variation decreases as **Figure 5(c)**, resulting in a reduction in the flow field's concentration at the concentration boundary tier. However, in **Figure 5(d)**, as the Schmidt number rises, the nanoparticle volume fraction does as well. The local skin friction coefficient, local Nusselt in conjunction with Sherwood numbers, and local nanoparticle Sherwood number compared with as a function of the streamwise distance *x* are illustrated throughout **Figure 6** to explore the implications of the Schmidt number on the flow field. **Figure 6(a)** illustrates the manner in which as predicted, an increase in the Schmidt number leads to decline in the local skin friction coefficient. Additionally, **Figure 6(b)** demonstrates that the local Nusselt number falls with a rise in the overall Schmidt number. However, as anticipated by **Figure 6(c)**, the local Sherwood number rises in the case of an elevated Schmidt number, in contrast to **Figure 6(d)**, the local nanoparticle Sherwood number drops as the Schmidt number rises.

6. Conclusions

This work adopts an evenly distributed magnetic field to explore hybrid effects employing varied convective flow via an inclined vertical porous plate in the presence of a porous medium. The results demonstrate that the fluid suction parameter and Schmidt number have an impact on the flow field. When the fluid suction is increased, the flow field's velocity, temperature, and concentration all decrease; on the other hand, the nanoparticle volume fraction decreases at $1.7 \le \eta \le 5$ and increases at $0 \le \eta < 1.7$. On the contrary, the general local Sherwood number rises while the local nanoparticle Sherwood number falls when the fluid suction component rises, whereas the local skin friction coefficient as well as the local Nusselt number all rise. The volume fraction of nanoparticles grows with increasing Schmidt number, despite the fact that the temperature, concentration, and velocity distributions of the flow field fall. With increasing Schmidt numbers, the local Sherwood number and skin friction coefficient rise, whereas the local Sherwood number for nanoparticles and the local Nusselt number decline.

The outcomes obtained from this investigation, in conjunction with data from physical science, will be beneficial to the engineering community, scholars, and

experimental scientists in discovering how nanofluid circulation operates in complex geometries. Additional investigations may be performed on broadening the features of nanofluid circulation over higher-level geometry, considering the current study has an extensive variety of significant implications. By considering the results of the present investigation, the drawbacks involving the present work can be explored for potential future studies in fields including three-dimensional nature flow, inconstant permeability in a medium of pores, and instability in conjunction with turbulent flow.

Conflicts of Interest

The authors declare no conflicts of interest regarding the publication of this paper.

References

[1] Buongiorno, J. (2005) Convective Transport in Nanofluids. *Journal of Heat Transfer*, **128**, 240-250. https://doi.org/10.1115/1.2150834

[2] Abu-Nada, E. (2008) Application of Nanofluids for Heat Transfer Enhancement of Separated Flows Encountered in a Backward Facing Step. *International Journal of Heat and Fluid Flow*, **29**, 242-249. https://doi.org/10.1016/j.ijheatfluidflow.2007.07.001

[3] Nield, D.A. and Kuznetsov, A.V. (2009) Thermal Instability in a Porous Medium Layer Saturated by a Nanofluid. *International Journal of Heat and Mass Transfer*, **52**, 5796-5801. https://doi.org/10.1016/j.ijheatmasstransfer.2009.07.023

[4] Nield, D.A. and Kuznetsov, A.V. (2009) The Cheng-Minkowycz Problem for Natural Convective Boundary-Layer Flow in a Porous Medium Saturated by a Nanofluid. *International Journal of Heat and Mass Transfer*, **52**, 5792-5795. https://doi.org/10.1016/j.ijheatmasstransfer.2009.07.024

[5] Ahmad, S. and Pop, I. (2010) Mixed Convection Boundary Layer Flow from a Vertical Flat Plate Embedded in a Porous Medium Filled with Nanofluids. *International Communications in Heat and Mass Transfer*, **37**, 987-991. https://doi.org/10.1016/j.icheatmasstransfer.2010.06.004

[6] Mittal, N., Manoj, V., Kumar, D.S. and Satheesh, A. (2012) Numerical Simulation of Mixed Convection in a Porous Medium Filled with Water/Al_2 O_3 Nanofluid. *Heat Transfer—Asian Research*, **42**, 46-59. https://doi.org/10.1002/htj.21029

[7] Mat Yasin, M.H., Arifin, N.M., Nazar, R., Ismail, F. and Pop, I. (2013) Mixed Convection Boundary Layer Flow Embedded in a Thermally Stratified Porous Medium Saturated by a Nanofluid. *Advances in Mechanical Engineering*, **5**, Article ID: 121943. https://doi.org/10.1155/2013/121943

[8] Gorla, R.S.R. and Hossain, A. (2013) Mixed Convective Boundary Layer Flow over a Vertical Cylinder Embedded in a Porous Medium Saturated with a Nanofluid. *International Journal of Numerical Methods for Heat & Fluid Flow*, **23**, 1393-1405. https://doi.org/10.1108/hff-03-2012-0064

[9] Saleh, M.H. (2013) Laminar Free Convection of Nanofluid Flow in Horizontal Porous Annulus. *World Academy of Science, Engineering and Technology*, **7**, 6-21.

[10] Uddin, Z. and Harmand, S. (2013) Natural Convection Heat Transfer of Nanofluids along a Vertical Plate Embedded in Porous Medium. *Nanoscale Research Letters*, **8**, Article No. 64. https://doi.org/10.1186/1556-276x-8-64

[11] Murthy, P.V.S.N., Sutradhar, A. and RamReddy, C. (2013) Double-diffusive Free Convection Flow Past an Inclined Plate Embedded in a Non-Darcy Porous Medium Saturated with a Nanofluid. *Transport in Porous Media*, **98**, 553-564. https://doi.org/10.1007/s11242-013-0160-z

[12] RamReddy, C. (2013) Influence of Viscous Dissipation on Free Convection in a Non-Darcy Porous Medium Saturated with Nanofluid in the Presence of Magnetic Field. *The Open Transport Phenomena Journal*, **5**, 20-29. https://doi.org/10.2174/1877729501305010020

[13] Aly, E.H. and Ebaid, A. (2013) New Analytical and Numerical Solutions for Mixed Convection Boundary-Layer Nanofluid Flow along an Inclined Plate Embedded in a Porous Medium. *Journal of Applied Mathematics*, **2013**, Article ID: 219486. https://doi.org/10.1155/2013/219486

[14] Yazdi, M.E., Moradi, A. and Dinarvand, S. (2013) MHD Mixed Convection Stagnation-Point Flow over a Stretching Vertical Plate in Porous Medium Filled with a Nanofluid in the Presence of Thermal Radiation. *Arabian Journal for Science and Engineering*, **39**, 2251-2261. https://doi.org/10.1007/s13369-013-0792-x

[15] Srinivasacharya, D. and Surender, O. (2014) Effect of Double Stratification on Mixed Convection Boundary Layer Flow of a Nanofluid Past a Vertical Plate in a Porous Medium. *Applied Nanoscience*, **5**, 29-38. https://doi.org/10.1007/s13204-013-0289-7

[16] El-Dawy, H.A., Mohammadein, A.A. and Gorla, R.S.R. (2014) Mixed Convection in a Nanofluid Past a Vertical Plate in a Saturated Porous Medium. *Journal of Nanofluids*, **3**, 117-120. https://doi.org/10.1166/jon.2014.1085

[17] Reddy, P.S. and Chamkha, A.J. (2016) Soret and Dufour Effects on MHD Convective Flow of Al_2O_3-Water and TiO_2-Water Nanofluids Past a Stretching Sheet in Porous Media with Heat Generation/absorption. *Advanced Powder Technology*, **27**, 1207-1218. https://doi.org/10.1016/j.apt.2016.04.005

[18] Khan, Z., Khan, I., Ullah, M. and Tlili, I. (2018) Effect of Thermal Radiation and Chemical Reaction on Non-Newtonian Fluid through a Vertically Stretching Porous Plate with Uniform Suction. *Results in Physics*, **9**, 1086-1095. https://doi.org/10.1016/j.rinp.2018.03.041

[19] Prasad, D.V.K., Chaitanya, G.S.K. and Raju, R.S. (2019) Double Diffusive Effects on Mixed Convection Casson Fluid Flow Past a Wavy Inclined Plate in Presence of Darcian Porous Medium. *Results in Engineering*, **3**, Article ID: 100019. https://doi.org/10.1016/j.rineng.2019.100019

[20] Uddin, M.N., Alim, M.A. and Rahman, M.M. (2019) MHD Effects on Mixed Convective Nanofluid Flow with Viscous Dissipation in Surrounding Porous Medium. *Journal of Applied Mathematics and Physics*, **7**, 968-982. https://doi.org/10.4236/jamp.2019.74065

[21] Falodun, B.O., Omowaye, A.J., Oyelami, F.H., Emadifar, H., Hamoud, A.A. and Atif, S.M. (2022) Double-Diffusive MHD Viscous Fluid Flow in a Porous Medium in the Presence of Cattaneo-Christov Theories. *Modelling and Simulation in Engineering*, **2022**, Article ID: 2533714. https://doi.org/10.1155/2022/2533714

[22] Raghunath, K., Ramana, R.M., Reddy, V.R. and Obulesu, M. (2023) Diffusion Thermo and Chemical Reaction Effects on Magnetohydrodynamic Jeffrey Nanofluid over an Inclined Vertical Plate in the Presence of Radiation Absorption and Constant Heat Source. *Journal of Nanofluids*, **12**, 147-156. https://doi.org/10.1166/jon.2023.1923

[23] Talbot, L., Cheng, R.K., Schefer, R.W. and Willis, D.R. (1980) Thermophoresis of Particles in a Heated Boundary Layer. *Journal of Fluid Mechanics*, **101**, 737-758. https://doi.org/10.1017/s0022112080001905

[24] Cebeci, T. and Bradshaw, P. (1984) Physical and Computational Aspects of Convective Heat Transfer. Springer.

[25] Nachtsheim, P.R. and Swigert, P. (1965) Satisfaction of Asymptotic Boundary Conditions in Numerical Solution of Systems of Nonlinear Equations of Boundary-Layer Type. NASA TND 3004.

[26] Reddy, M.G. and Reddy, N.B. (2011) Mass Transfer and Heat Generation Effects on MHD Free Convection Flow Past an Inclined Vertical Surface in a Porous Medium. *Journal of Applied Fluid Mechanics*, **4**, 7-11.